Cardiovasc Eng
DOI 10.1007/s10558-008-9057-9

ORIGINAL PAPER

Development and Application of a Logistic-Based Systolic Model for Hemodynamic Measurements Using the Esophageal Doppler Monitor

Glen M. Atlas

Abstract The esophageal Doppler monitor (EDM) is a clinically useful device for minimally invasive assessment of cardiac output, preload, afterload, and contractility. An empirical model, based upon the logistic function, has been developed. Use of this model illustrates how the EDM could estimate the net effect of aortic and non-aortic contributions to inertia, resistance, and elastance within real time. This is based on an assumed mechanical impedance conceptually resembling that of a series arrangement of a spring, mass, and dashpot. In addition, when used with an invasive radial arterial catheter, the EDM may also estimate aortic pulse wave velocity, as well as aortic characteristic impedance, and characteristic volume. Approximations of left ventricular stroke work and stroke power can also be made. Furthermore, the effects of inertia, resistance, and elastance, on mean blood pressure during systole, can be quantified. These additional parameters could offer insight for clinicians, as well as researchers, and may be beneficial in further examining and utilizing clinical hemodynamics with the EDM. These additional measurements also underscore the need to integrate the EDM with existing and future monitoring equipment.

G. M. Atlas (✉)
Department of Anesthesiology, University of Medicine and Dentistry of New Jersey, New Jersey Medical School, Newark, NJ, USA
e-mail: atlasgm@umdnj.edu

G. M. Atlas
Department of Chemistry, Chemical Biology & Biomedical Engineering, Stevens Institute of Technology, Hoboken, NJ, USA

G. M. Atlas
Department of Biomedical Engineering, Rutgers University, Piscataway, NJ, USA

Keywords Esophageal doppler · Hemodynamic model · Logistic

Introduction

The esophageal Doppler monitor (EDM) offers clinicians, both rapid and safe cardiovascular assessment in real time. Historically, evaluation of hemodynamic parameters has been commonly done with a pulmonary artery occlusion [Swan-Ganz] catheter. These catheters are highly invasive and fraught with potential life-threatening complications (Domino et al. 2004; Vincent et al. 1998) which are summarized in Table 1 (American Society of Anesthesiologists Task Force on Guidelines for Pulmonary Artery 2003). Additionally, the accuracy of the data, derived from these catheters, can be flawed by coexisting diseases, misinterpretation, and other conditions (American Society of Anesthesiologists Task Force on Guidelines for Pulmonary Artery 2003; Rothenberg and Tuman 2000). Furthermore, in spite of the tremendous risks associated with the pulmonary artery occlusion catheter, no significant benefit from these devices has been conclusively and consistently demonstrated through multiple large-scale patient-based outcome studies (American Society of Anesthesiologists Task Force on Guidelines for Pulmonary Artery 2003; Polanczyk et al. 2001; Warzawski and Deye 2003; Sandham and Hull 2003; The National Heart, Lung, and Blood ARDS Clinical Trials Network 2006).

Transesophageal echocardiography (TEE) can also be used to assess hemodynamic status. However, this requires expensive technology as well as some significant training. Furthermore, the TEE probe is considerably larger than those probes associated with the EDM.

Table 1 Complications, and their incidence, associated with pulmonary artery occlusion catheters (American Society of Anesthesiologists Task Force on Guidelines for Pulmonary Artery 2003)

Complication	Incidence in most studies (%)
Arterial puncture	≤3.6
Pneumothorax	0.3–1.9
Minor dysrthymias	>20
Severe dysrhymias (ventricular tachycardia or fibrillation)	0.3–3.8
Pulmonary artery rupture	0.03–0.7
Positive catheter-tip cultures	≤19
Catheter-related sepsis	0.7–3.0
Venous thrombosis	0.5–3.0
Pulmonary infarction	0.1–2.6
Valvular/endocardial vegetations or endocarditis	2.2–7.1

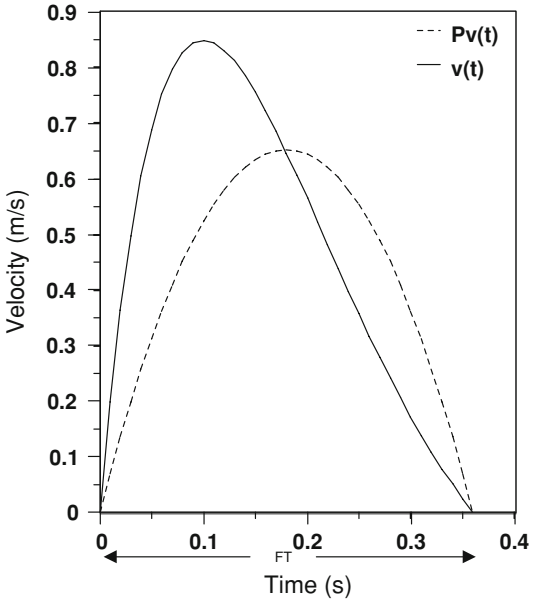

Fig. 1 Velocity of pulmonary blood flow, $Pv(t)$, and aortic blood flow, $v(t)$, as a function of time. These graphs were generated using the logistic-based systolic model. Flow time, FT, represents left ventricle ejection time

The major advantage of TEE, over other devices, is its ability, using imaging, to visualize and assess cardiac anatomy and associated dynamic wall and valvular changes (Vignon 2005). However, TEE can only be used on an intermittent basis. This is due to the large size of its probe. Whereas the EDM, with its significantly smaller probe, can be used for an extended period of time (English and Moppett 2005). It should be noted that the EDM measures only distal aortic blood flow velocity.

With the EDM, preload can be assessed by examination of corrected flow time, FTc (Singer and Bennett 1991; DiCorte et al. 2000; Feldman et al. 2004; Seoudi et al. 2003; Gan et al. 2002). Clinically, FTc correlates with preload as measured with a pulmonary artery occlusion [Swan-Ganz] catheter (Madan et al. 1999). The relationship between flow time (FT) and FTc is based upon heart rate (HR) in beats per minute: $\mathrm{FT} = \mathrm{FTc}\sqrt{60/\mathrm{HR}}$ where FT represents left ventricle ejection time during systole. This is illustrated in Fig. 1.

In addition, FTc has been shown to correlate better with left ventricular (LV) end-diastolic area than pulmonary artery occlusion pressure (DiCorte et al. 2000). Stroke volume (SV), as measured with the EDM, can also be used to assess preload (Roeck et al. 2003). However, changes in contractility and flow time have to taken into account when using this parameter (Kumar et al. 2004) (See Appendix A). Furthermore, it appears that low stroke volume, when measured with an EDM, may also have prognostic value following cardiac surgery (Poeze et al. 1999).

With the EDM, contractility is readily quantified by examining peak velocity and acceleration of distal aortic blood flow. In addition, that portion of cardiac output (CO), which is measured in the distal aorta, is continuously assessed by determining the product of distal aortic diameter and the velocity of descending aortic blood flow. A correction, based upon a linear regression, of the blood flow in the distal aorta, is then used to determine *total* cardiac output (See Appendix A) (Boulnois and Pechoux 2000; Dark and Singer 2004; Valtier et al. 1998; Lafanechere et al. 2006).

Furthermore, distal aortic diameter can be directly measured using an M-mode function such as that available on the Arrow Hemosonic® EDM. This feature also helps to focus the ultrasound *directly* on the aorta thus assuring that the angle of the Doppler signal is correct. Consequently, diameter and velocity are accurately and continuously assessed (Boulnois and Pechoux 2000).

Afterload can also be clinically measured with the EDM. This is accomplished by calculating: $\mathrm{TSVR} = \mathrm{MAP}/\mathrm{CO}$ where TSVR represents aortic characteristic resistance. MAP is mean arterial blood pressure which can be measured either noninvasively, with a blood pressure cuff, or invasively with an indwelling arterial catheter and transducer. Typically, the clinician will input the mean arterial pressure into the EDM. Following this, the EDM will then calculate TSVR.

Central venous pressure (CVP), if available, can also be used to calculate SVR using the same formula as a one would use with a pulmonary artery occlusion or CVP catheter: $\mathrm{SVR} = \frac{\mathrm{MAP}-\mathrm{CVP}}{\mathrm{CO}}$.

The EDM is typically placed orally in anesthetized patients whose trachea is intubated. Nasal placement, in awake patients, has also been described. This represents a distinct advantage of the EDM over TEE (English and

Moppett 2005; Atlas and Mort 2001; Levy 2001; Dodd 2002).

This paper examines additional "new" measurements with the EDM. These include hemodynamic assessments of inertia, resistance, and elastance conceptually resembling a net series arrangement of a spring, mass, and dashpot (Nichols and O'Rourke 2005). To exemplify this, a logistic-based systolic model is developed and applied to distal aortic blood flow. Means of estimating aortic pulse wave velocity, as well as aortic elastance, characteristic volume, and characteristic impedance are also examined. Furthermore, evaluations of both left ventricular stroke work and stroke power can be made. Also, the individual effects, of inertia, resistance, and elastance, on mean blood pressure during systole, can be assessed. These additional measurements depend upon the EDM ultimately being integrated with existing OR and ICU monitors.

Development of a Logistic-Based Systolic Model

Pulmonary Circulation and Flow Time

By using a model whose form is similar to the logistic function (Beltrami 1987), $Pv(t)$, the velocity of pulmonary artery blood flow, can be represented as a parabola-like function occuring over the course of ventricular ejection time or flow time:

$$Pv(t) = \alpha\left[\left(1 - \frac{t}{\mathrm{FT}}\right)t\right]. \quad 0 \le t \le \mathrm{FT} \tag{1}$$

where α is an acceleration term with a value of about 7.25 m s^{-2}. Clinically, in humans with normal cardiac function, the velocity of pulmonary artery blood flow has been observed to be age-independent (Gardin et al. 1987). A plot of $Pv(t)$ is shown in Fig. 1.

FT represents flow time, during systole, or left ventricle ejection time. Corrected flow time, FTc, has a normal range of 330–360 and is "expressed" in terms of milliseconds. In addition, FT is age-independent whereas FTc increases with age (Gardin et al. 1987).

For computational purposes, both left and right ventricular ejection times (flow time or FT) are assumed to be equal. In addition, this model is only applicable during systole: $0 \le t \le \mathrm{FT}$.

It should be noted that the EDM does not *directly* measure right heart function. However, changes in right heart function may ultimately be detected as changes in the velocity of distal aortic blood flow.

In this model, displacement, as a function of time, also maintains the familiar logistic sigmoid character (See Appendix B). Logistic-based modeling has also been used in other cardiovascular settings (Matsubara et al. 1995).

Systemic Circulation

Equation (1), for pulmonary artery velocity, can be modified to accommodate the "pumping effects" of the left ventricle:

$$v(t) = \alpha\beta e^{-\gamma t}\left[\left(1 - \frac{t}{\mathrm{FT}}\right)t\right]. \quad 0 \le t \le \mathrm{FT} \tag{2}$$

where $v(t)$ represents the velocity of distal aortic blood flow. The peak value for distal aortic blood flow velocity has been shown to have an age-dependent normal range (Mowat et al. 1983).

β is dimensionless. It has an age-dependent range from approximately 1.5 to 3.2 and can be thought of as a "gain" similar to that of an amplifier. This "time-dependent and age-dependent velocity amplifier" concept is further illustrated in Fig. 2. $v(t)$ is illustrated in Figs. 1 and 3.

The time at which *peak* distal aortic blood flow velocity occurs, t_{pv}, is approximately 0.1 ms (Gardin et al. 1987). This also appears to be clinically constant and age-independent in normal humans (Gardin et al. 1987).

A solution for γ can be obtained so that $v(t)$ has its peak, or maximum value, at t_{pv}. This can be obtained by solving for γ with $a(t) = \mathrm{d}v(t)/\mathrm{d}t = 0$ at $t = t_{pv} = 0.1$ s. (See "Acceleration of Aortic Blood Flow" section). Note that t_{pv} is also when acceleration is 0:

$$\alpha\beta \mathrm{e}^{-\gamma \cdot t_{pv}}\left[\gamma\left(\frac{t_{pv}}{\mathrm{FT}} - 1\right)t_{pv} - 2\frac{t_{pv}}{\mathrm{FT}} + 1\right] = 0. \tag{3}$$

which can be expressed as:

$$\gamma\left(\frac{t_{pv}}{\mathrm{FT}} - 1\right)t_{pv} - 2\frac{t_{pv}}{\mathrm{FT}} + 1 = 0. \tag{4}$$

In addition, β does not appear in (4). Thus, in this model, the t_{pv} is independent of age. Therefore, this model

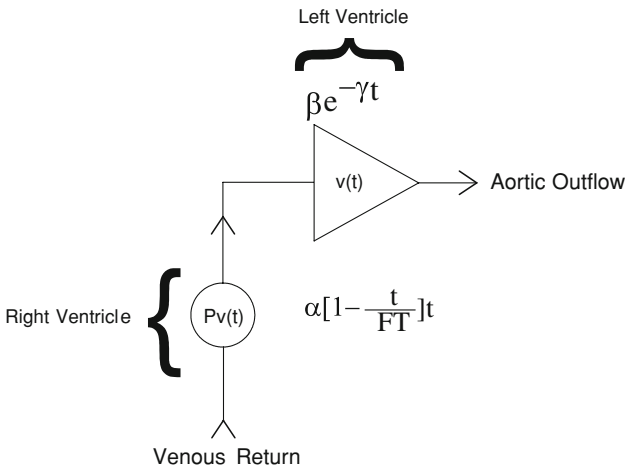

Fig. 2 The velocity of aortic blood flow, as measured with an esophageal Doppler monitor (EDM), can be modeled with the right ventricle as an "age-independent" velocity source and the left ventricle as an "age-dependent and time-dependent" velocity amplifier

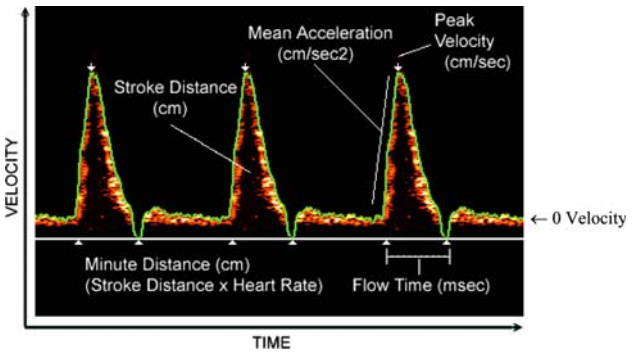

Fig. 3 Velocity versus time waveform for a typical EDM signal. Note the location of zero velocity along the ordinate

maintains age-independence for time to peak velocity. It should also be noted that α does not appear in the above formula and that t_{pv}, in the distal aorta, can be modeled independently of pulmonary artery blood flow.

Solving (4) for γ yields:

$$\gamma = \frac{2 - \frac{\mathrm{FT}}{t_{pv}}}{t_{pv} - \mathrm{FT}}. \tag{5}$$

γ is then calculated as 6.154 s^{-1}. This is based on $t_{pv} = 0.1$ and a FT = 360 ms.

Clinically, a reduction in left ventricular contractility can be observed as a greater t_{pv} as well as a decrease in acceleration and/or peak velocity (DuBourg et al. 1993, Wallmeyer et al. 1986). With this model, an increase in t_{pv} is observed as a decrease in the value of γ:

$$\lim_{t_{pv} \to \frac{\mathrm{FT}}{2}} \gamma = \lim_{t_{pv} \to \frac{\mathrm{FT}}{2}} \frac{2 - \frac{\mathrm{FT}}{t_{pv}}}{t_{pv} - \mathrm{FT}} = 0. \tag{6}$$

Acceleration of Distal Aortic Blood Flow

Acceleration of distal aortic blood flow is also clinically useful in assessing left ventricular contractility (DuBourg et al. 1993) and is readily determined with the EDM. It can be modeled by differentiating (2) with respect to time:

$$\frac{\mathrm{d}v(t)}{\mathrm{d}t} = a(t) = \alpha\beta \mathrm{e}^{-\gamma t}\left[\gamma\left(\frac{t}{\mathrm{FT}} - 1\right)t - 2\frac{t}{\mathrm{FT}} + 1\right]. \tag{7}$$

Age-dependent normal values, for acceleration of distal aortic blood flow, have also been clinically determined (Mowat et al. 1983). As shown in Figs. 1 and 3, the steepest aspect of the distal aortic blood flow velocity curve occurs during the early portion of systole.

Stroke Distance

Stroke distance within the aorta, $\mathrm{SD}_{\mathrm{aorta}}$, is analogous to mechanical displacement. By assessing the integral, of velocity over flow time, this function can be modeled as a *definite* integral:

$$\mathrm{SD}_{\mathrm{aorta}} = \int_0^{\mathrm{FT}} v(t)\mathrm{d}t = \int_0^{\mathrm{FT}} \alpha\beta \mathrm{e}^{-\gamma t}\left[\left(1 - \frac{t}{\mathrm{FT}}\right)t\right]\mathrm{d}t. \tag{8}$$

The solution of (8) is (See Appendix B):

$$\mathrm{SD}_{\mathrm{aorta}} = \left[\left(1 + \frac{2}{\mathrm{FT}\gamma}\right)\mathrm{e}^{-\gamma \mathrm{FT}} - \left(-1 + \frac{2}{\mathrm{FT}\gamma}\right)\right]\frac{\alpha\beta}{\gamma^2} \tag{9}$$

Minute distance is defined as the product of stroke distance and heart rate and correlates with cardiac output (See Appendix A). In addition, stroke distance can be modeled as a function of time. This would be determined using an *indefinite* integral (See "Estimating Inertia, Resistance, and Elastance in the Time Domain" Section).

Furthermore, stroke volume within the distal aorta, $\mathrm{SV}_{\mathrm{aorta}}$, is the product of $\mathrm{SD}_{\mathrm{aorta}}$ and distal aortic cross sectional area (See Appendix A).

Peak Distal Aortic Blood Flow Velocity as a Function of Corrected Flow Time

Based upon the Frank–Starling mechanism, within a normal range of preload, left ventricle ejection, or cardiac output, is proportional to preload.

Using EDM-based parameters, peak distal aortic blood flow velocity, v_{peak}, was found to be proportional, in an approximately linear manner, to corrected flow time, FTc, in normal humans (Singer et al. 1991). Similarly, in humans (Kumar et al. 2004), as well as in animals (Hsieh et al. 1991), contractility increases with increasing preload.

The logistic-based systolic model illustrates this relationship. By keeping HR, t, and γ fixed and replacing FT with the expression for FTc, (2) can be expressed as:

$$V_{\mathrm{peak}}(\mathrm{FTc}) = \alpha\beta \mathrm{e}^{-\gamma t_{pv}}\left(1 - \frac{t_{pv}}{\mathrm{FTc}\sqrt{\frac{60}{\mathrm{HR}}}}\right)t_{pv}. \tag{10}$$

Plotting $v_{\mathrm{peak}}(\mathrm{FTc})$ versus FTc, as shown in Fig. 4, a near-linear relationship between peak aortic blood flow velocity and FTc can be observed. Flow-based observations made in vivo behave similarly (Singer and Bennett 1991; Singer et al. 1991; Hsieh et al. 1991).

It should also be noted that decreases in afterload can also result in slight increases in FTc (Singer and Bennett 1991; Singer et al. 1991). In these situations, assessment of stroke volume and/or other clinical measurements may be necessary to evaluate fluid status. Furthermore, assessment of "characteristic volume" may prove to be useful under these circumstances. (See "Pulse Wave Velocity, Characteristic Volume and Characteristic Impedance" section).

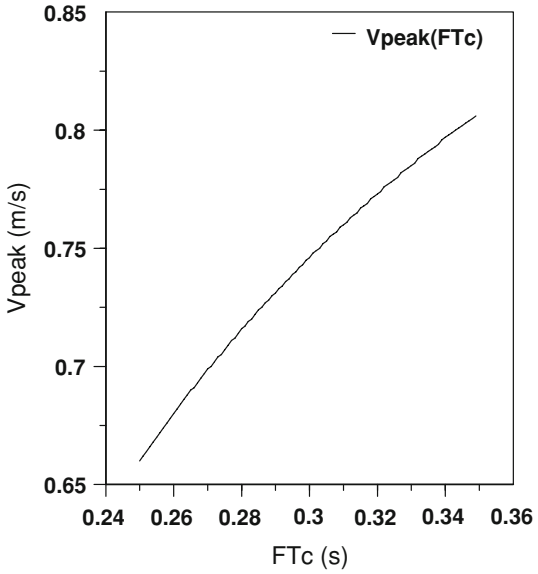

Fig. 4 Peak velocity of aortic blood flow as a function of corrected flow time, FTc. In vivo measurements resemble this relationship (Singer et al. 1991)

Application of the Logistic-Based Systolic Model

Estimating Inertia, Resistance, and Elastance in the Time Domain

Using the logistic-based systolic model as an example, time-domain based estimates of the hemodynamic characteristics of inertia (L), resistance (R), and elastance ($1/C$) can be made with an EDM. This is done by assuming an impedance which conceptually resembles a series arrangement of a spring, mass, and dashpot (Nichols and O'Rourke 2005) and applying the aforementioned aortic velocity function:

$$p(t) = A\left\{L \cdot \frac{\mathrm{d}v(t)}{\mathrm{d}t} + R \cdot v(t) + \frac{1}{C} \cdot \int v(t)\mathrm{d}t\right\}. \quad 0 \le t \le \mathrm{FT}. \tag{11}$$

Note that A represents distal aortic cross sectional area. This is based upon $A = \pi r^2$ where r is distal aortic radius. *Equation (11) is not meant to be an oscillator*. Rather, the logistic-based model functions as a single cardiac systolic cycle or "one shot."

It should be realized that inertia, resistance and elastance can be represented as the net effect of their aortic and non-aortic components. This is illustrated in Fig. 5. In addition, $p(t)$ represents a peripheral blood pressure. This would generally be obtained using a radial arterial catheter.

Again, velocity is:

$$v(t) = \alpha\beta \mathrm{e}^{-\gamma t}\left[\left(1 - \frac{t}{\mathrm{FT}}\right)t\right]. \quad 0 \le t \le \mathrm{FT} \tag{12}$$

and acceleration:

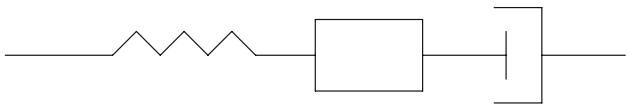

Fig. 5 The net effect of aortic and non-aortic contributions to inertia, resistance, and elastance. This conceptually resembles a series arrangement of a spring, mass, and dashpot

$$\frac{\mathrm{d}v(t)}{\mathrm{d}t} = a(t) = \alpha\beta \mathrm{e}^{-\gamma t}\left[\gamma\left(\frac{t}{\mathrm{FT}} - 1\right)t - 2\frac{t}{\mathrm{FT}} + 1\right]. \tag{13}$$

Stroke distance or displacement, as a function of time, is represented by the *indefinite* integral of velocity over time (See Appendix B):

$$\begin{aligned}\int v(t)\mathrm{d}t &= sd(t) \\ &= \left[\left[\left(\frac{t}{\mathrm{FT}} - 1\right)t + \left(2\frac{t}{\mathrm{FT}} - 1\right)\frac{1}{\gamma} + \frac{2}{\mathrm{FT}\gamma^2}\right]\frac{\alpha\beta}{\gamma}\mathrm{e}^{-\gamma t}\right] \\ &\quad - \left(-1 + \frac{2}{\mathrm{FT}\gamma}\right)\frac{\alpha\beta}{\gamma 2}.\end{aligned} \tag{14}$$

where the *constant of integration* $= (-1 + \frac{2}{\mathrm{FT}\gamma})\frac{\alpha\beta}{\gamma^2}$ so that $\mathrm{sd}(0) = 0$. Thus, at $t = 0$, displacement is zero. Note that the constant of integration is *subtracted*.

The following system of equations can then be expressed in matrix form:

$$A \cdot \begin{bmatrix} a(0) & v(0) & sd(0) \\ a(t_{pv}) & v(t_{pv}) & sd(t_{pv}) \\ a(\mathrm{FT}) & v(\mathrm{FT}) & sd(FT) \end{bmatrix}\begin{bmatrix} L \\ R \\ \frac{1}{C} \end{bmatrix} = \begin{bmatrix} p(0) \\ p(t_{pv}) \\ p(FT) \end{bmatrix}. \tag{15}$$

Note that: $v(0) = sd(0) = v(\mathrm{FT}) = a(t_{pv}) = 0$.
Furthermore:

$$\begin{aligned} p(0) &= \text{radial arterial pressure at end-diastole} \\ &= \text{radial arterial pressure at start-systole} \end{aligned} \tag{16}$$

$$p(t_{pv}) = \text{radial arterial pressure at peak aortic blood flow velocity} \tag{17}$$

$$\begin{aligned} p(\mathrm{FT}) &= \text{radial arterial pressure at end-systole} \\ &= \text{radial arterial pressure at start-diastole.} \end{aligned} \tag{18}$$

Using Cramer's rule or matrix inversion (Kreyszig 1999), (15) can be solved and values for L, R, and $1/C$ can be determined (See "A Numerical Example" section):

$$\begin{bmatrix} L \\ R \\ \frac{1}{C} \end{bmatrix} = \frac{1}{A}\left\{\begin{bmatrix} a(0) & v(0) & sd(0) \\ a(t_{pv}) & v(t_{pv}) & sd(t_{pv}) \\ a(\mathrm{FT}) & v(\mathrm{FT}) & sd(FT) \end{bmatrix}^{-1}\begin{bmatrix} p(0) \\ p(t_{pv}) \\ p(FT) \end{bmatrix}\right\}. \tag{19}$$

Thus, the net effect of aortic and non-aortic contributions to L, R, and $1/C$ can then be estimated, in real-time, with simultaneous EDM-based technology and a radial arterial catheter.

Furthermore, alternative numerical techniques and methods, other than the logistic-based systolic model, could be used to determine the acceleration, velocity, and stroke distance terms for (19). This would include values obtained directly from the EDM and a radial arterial catheter. Values for Eq. (19) could also be obtained by signal averaging and other processing techniques to reduce the effect of any aberrant information. Equation (19) could then be used on an almost instantaneous basis thus enabling near "beat-to-beat" hemodynamic calculations.

Thus, the net effect of the aorto-radial components of inertia, resistance and elastance could be obtained, with the EDM, in conjunction with values for $p(0)$, $p(t_{pv})$, and $p(\mathrm{FT})$. Following this, $p(t)$ can be approximated with (11). As shown in the following section, $p(t)$ can also be determined using a Laplace transform method.

Reasonable approximations may also be obtained with a noninvasive blood pressure cuff used in conjunction with an EDM. In addition, the pressure at peak systole, $p(t_{\mathrm{sys\_peak}})$, could be used instead of $p(t_{pv})$. This would necessitate using appropriate values for acceleration, velocity, and stroke distance which would be obtained at $t = t_{\mathrm{sys\_peak}}$.

Figure 6 graphically illustrates the relationship between $p(t)$ and $v(t)$.

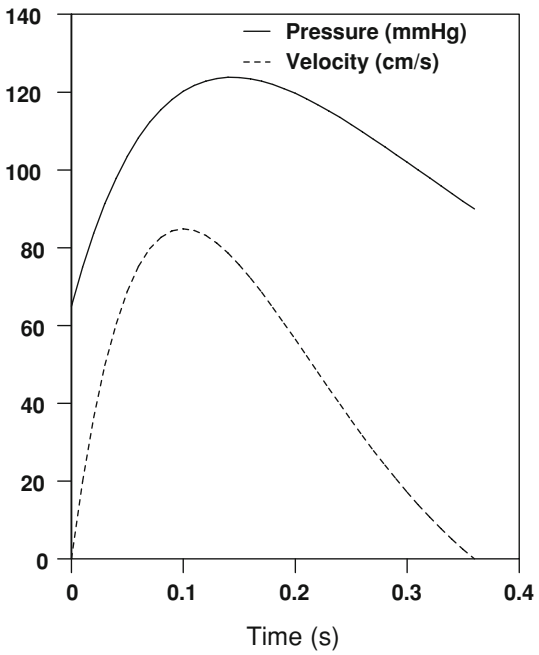

Fig. 6 Peripheral blood pressure, and distal aortic blood flow velocity, as a function of time during systole. The velocity curve is derived using EDM-based parameters and the logistic-based systolic model. Following this, inertia (L), resistance (R) and elastance ($1/C$) are determined using (11) and systolic pressures: $p(0)$, $p(t_{pv})$, and $p(\mathrm{FT})$. Pressure, as a function of time during systole, is then determined with either Eq. (11) or (28)

Examining Aortic $p(t)$ and $\mathrm{d}p/\mathrm{d}t$

The time rate change of aortic pressure, aortic $\mathrm{d}p/\mathrm{d}t$, can also be investigated with the EDM. This can be illustrated with the logistic-based systolic model using the previously determined method to obtain values for inertia, resistance, and elastance. In addition, the time at which peak aortic pressure occurs, when $\mathrm{d}p/\mathrm{d}t = 0$, can also be found. Clinically, "time to peak pressure" has also been examined when assessing overall aortic impedance (Mitchell et al. 2003).

To facilitate this, aortic $\mathrm{d}p/\mathrm{d}t$ can be determined, from radial artery $\mathrm{d}p/\mathrm{d}t$, using transfer functions (Pauca et al. 2001). Similarly, radial artery tonometers have been used to accurately assess aortic pressure (Chen et al. 1997).

Evaluating maximum aortic $\mathrm{d}p/\mathrm{d}t$ is clinically helpful for the management of aortic dissections (Carney et al. 1975; Prokop et al. 1970) and may be a useful cardiac index as well (Schertel 1998; De Hert et al. 2006). Also, maximum aortic dp/dt can be determined using the product of blood density, aortic pulse wave velocity, and the maximum acceleration of aortic blood flow (Atlas 2002) (See "Pulse Wave Velocity, Characteristic Volume and Aortic Characteristic Impedance" section). The EDM may also be used to clinically assess maximum aortic $\mathrm{d}p/\mathrm{d}t$ using known, or assumed, values for aortic pulse wave velocity and blood density (Atlas 2002).

This analysis of this model is accomplished by first transforming $p(t)$ into the complex Laplace domain, $P(s)$, which consists of both real and imaginary components within the frequency domain. Subsequently, rearrangement into partial fractions collects "like" terms within the Laplace domain. The inverse Laplace transform then yields an expression for $p(t)$ which can be readily differentiated with respect to time. In addition, differentiation can be done directly in the Laplace domain (Kreyszig 1999). Table 2 illustrates the pertinent Laplace transforms for the analysis of this model (Kreyszig 1999).

Thus, using Table 2, the Laplace transform, of the resistance term from (11), is:

Table 2 Applicable Laplace transforms (Kreyszig 1999)

Laplace domain $P(s)$	Time domain $p(t)$	Comment
$\frac{1}{(s+\gamma)^n}$	$\left[\frac{t^{n-1}}{(n-1)!}\right]\mathrm{e}^{-\gamma t}$	$n = 1, 2, 3\ldots$
$\frac{k}{s}$	k	$k =$ Constant
1	$\delta(t)$	$\delta(t) =$ Dirac delta function
$sP(s) - p(0)$	$\mathrm{d}p(t)/\mathrm{d}t$	First derivative

$$\mathscr{L}(A \cdot R \cdot v(t)) = \frac{-\alpha\beta AR}{\mathrm{FT}}\left[\frac{-\mathrm{FT}}{(s+\gamma)^2} + \frac{2}{(s+\gamma)^3}\right]. \tag{20}$$

whereas the Laplace transform of the inertia term is:

$$\mathscr{L}(A \cdot L \cdot a(t)) = \frac{\alpha\beta \mathrm{AL}}{\mathrm{FT}}\left[\frac{\mathrm{FT}}{(S+\gamma)} - \frac{(2+\gamma\mathrm{FT})}{(S+\gamma)^2} + \frac{2\gamma}{(S+\gamma)^3}\right]. \tag{21}$$

And that of the elastance term is:

$$\mathscr{L}\left(A \cdot \frac{1}{C} \cdot sd(t)\right) = \frac{\alpha\beta A}{C\gamma^3\mathrm{FT}}\left[\frac{2-\mathrm{FT}\gamma}{(s+\gamma)} + \frac{(2-\mathrm{FT}\gamma)\gamma}{(s+\gamma)^2} + \frac{2\gamma^2}{(s+\gamma)^3}\right] - \left(-1 + \frac{2}{\mathrm{FT}\gamma}\right)\frac{\alpha\beta A}{\gamma^2 Cs}. \tag{22}$$

Addition and partial fraction rearrangement, of the above Laplace transforms from (20–22), yields:

$$P(s) = \frac{\Phi}{(s+\gamma)} + \frac{\Psi}{(s+\gamma)^2} + \frac{2\Omega}{(s+\gamma)^3} - \frac{K}{s}. \tag{23}$$

where:

$$\Phi = \alpha\beta A\left[L - \frac{1}{\gamma^2 C} + \frac{2}{C\gamma^3\mathrm{FT}}\right] \tag{24}$$

$$\Psi = \alpha\beta A\left[R - \gamma L - \frac{2L}{\mathrm{FT}} - \frac{1}{\gamma C} + \frac{2}{C\gamma^2\mathrm{FT}}\right] \tag{25}$$

$$\Omega = \frac{\alpha\beta A}{\mathrm{FT}}\left[-R + \gamma L + \frac{1}{\gamma C}\right] \tag{26}$$

$$K = \frac{\alpha\beta A}{\gamma^2 C}\left[-1 + \frac{2}{\gamma\mathrm{FT}}\right]. \tag{27}$$

The inverse Laplace transform of (23) is $\mathscr{L}^{-1}(P(s)) = p(t)$:

$$p(t) = \mathrm{e}^{-\gamma t}\left[\Phi + \Psi t + \Omega t^2\right] - K. \quad 0 \le t \le \mathrm{FT} \tag{28}$$

Thus, $p(t)$ can be expressed as a function of L, R, and $1/C$ and with the coefficients from the logistic-based systolic model. Note that $p(t)$, from (28), is numerically identical to $p(t)$ from (11).

From (28), $\mathrm{d}p/\mathrm{d}t$ can be readily determined:

$$\frac{\mathrm{d}p}{\mathrm{d}t} = \mathrm{e}^{-\gamma t}\left[-\gamma(\Phi + \Psi t + \Omega t^2) + (\Psi + 2\Omega t)\right]. \tag{29}$$

The time to peak systolic pressure occurs at $t = t_{\mathrm{sys\_peak}}$ when $\mathrm{d}p/\mathrm{d}t = 0$. It can be determined by setting (29) equal to zero and solving the resultant quadratic:

$$t_{\mathrm{sys\_peak}} = \frac{-\gamma\Psi + 2\Omega + \sqrt{\gamma^2\left[\Psi^2 - 4\Phi\Omega\right] + 4\Omega^2}}{2\gamma\Omega}. \tag{30}$$

Of note, only the positive square root of (30) results in a meaningful value for $t_{\mathrm{sys\_peak}}$.

The Laplace transform itself can also be used to determine $\mathrm{d}p/\mathrm{d}t$. This can be done with the following relationship (Kreyszig 1999):

$$\mathscr{L}(\mathrm{d}p/\mathrm{d}t) = sP(s) - p(0). \tag{31}$$

Using (28), $p(0)$ is found to be:

$$p(0) = \Phi - K. \tag{32}$$

So that (31) can now be expressed as:

$$\mathscr{L}(\mathrm{d}p/\mathrm{d}t) = sP(s) - p(0) = \frac{s\Phi}{(s+\gamma)} + \frac{s\Psi}{(s+\gamma)^2} + \frac{2s\Omega}{(s+\gamma)^3} - \Phi. \tag{33}$$

The inverse Laplace transform of (33) yields:

$$\mathrm{d}p/\mathrm{d}t = \Phi[\delta(t) - \gamma\mathrm{e}^{-\gamma t}] + \Psi\mathrm{e}^{-\gamma t}[1 - \gamma t] + 2\Omega\mathrm{e}^{-\gamma t}\left[\frac{-1}{2}\gamma t^2 + t\right] - \Phi\delta(t). \tag{34}$$

Note that $\Phi\delta(\mathrm{t})$, the product of Φ and the *Dirac delta function* (Kreyszig 1999), cancels within (34). Equation 34 then reduces to the same as (29):

$$\mathrm{d}p/\mathrm{d}t = \mathrm{e}^{-\gamma t}\left[-\Omega\gamma t^2 + [2\Omega - \Psi\gamma]t - \Phi\gamma + \Psi\right]. \tag{35}$$

The solution to (35) is identical, for $t = t_{sys\_peak}$ as in (29), when $\mathrm{d}p/\mathrm{d}t = 0$.

The numerical values for coefficients Φ, Ψ, Ω, K can also be readily verified. This is accomplished by expanding (28) using a matrix format and examining four distinct values, for pressure, occurring during systole:

$$\begin{bmatrix} 1 & 0 & 0 & -1 \\ \mathrm{e}^{-\gamma t_1} & t_1\mathrm{e}^{-\gamma t_1} & t_1^2\mathrm{e}^{-\gamma t_1} & -1 \\ \mathrm{e}^{-\gamma t_2} & t_2\mathrm{e}^{-\gamma t_2} & t_2^2\mathrm{e}^{-\gamma t_2} & -1 \\ \mathrm{e}^{-\gamma t_3} & t_3\mathrm{e}^{-\gamma t_3} & t_3^2\mathrm{e}^{-\gamma t_3} & -1 \end{bmatrix}\begin{bmatrix} \Phi \\ \Psi \\ \Omega \\ \mathrm{K} \end{bmatrix} = \begin{bmatrix} p(0) \\ p(t_1) \\ p(t_2) \\ p(t_3) \end{bmatrix}. \tag{36}$$

Thus:

$$\begin{bmatrix} \Phi \\ \Psi \\ \Omega \\ \mathrm{K} \end{bmatrix} = \begin{bmatrix} 1 & 0 & 0 & -1 \\ \mathrm{e}^{-\gamma t_1} & t_1\mathrm{e}^{-\gamma t_1} & t_1^2\mathrm{e}^{-\gamma t_1} & -1 \\ \mathrm{e}^{-\gamma t_2} & t_2\mathrm{e}^{-\gamma t_2} & t_2^2\mathrm{e}^{-\gamma t_2} & -1 \\ \mathrm{e}^{-\gamma t_3} & t_3\mathrm{e}^{-\gamma t_3} & t_3^2\mathrm{e}^{-\gamma t_3} & -1 \end{bmatrix}^{-1}\begin{bmatrix} p(0) \\ p(t_1) \\ p(t_2) \\ p(t_3) \end{bmatrix}. \tag{37}$$

Pulse Wave Velocity, Characteristic Volume, and Characteristic Impedance

Aortic pulse wave velocity, v_{pw}, has been shown to increase in the presence of renal failure (Blacher et al. 1999), aging (Bulpitt et al. 1999; Rogers et al. 2001), Marfan's disease (Groenink et al. 1998), atherosclerosis (Hopkins et al. 1994; Lehmann 1999), and hypertension (McEniery et al. 2005). Traditionally, pulse wave velocity is described with the Moens–Korteweg equation (Milnor 1989) (See Appendix C). Furthermore, v_{pw} is related to

dp/dt, blood density, and acceleration (Atlas 2002; Sugawara et al. 1994):

$$\frac{\mathrm{d}p}{\mathrm{d}t} = \rho v_{pw} a(t). \tag{38}$$

Examining the above equation at the start of systole, when $t = 0$, yields:

$$\frac{\frac{\mathrm{d}p}{\mathrm{d}t}|_{t=0}}{\rho \cdot a(0)} = v_{pw}. \tag{39}$$

Substitution of $\frac{\mathrm{d}p}{\mathrm{d}t}|_{t=0}$ from (29) or (35), and $a(0)$ from (13), yields:

$$\frac{\frac{\mathrm{d}p}{\mathrm{d}t}|_{t=0}}{\rho \cdot a(0)} = \frac{-\gamma\Phi + \Psi}{\rho\beta\alpha} = v_{pw}. \tag{40}$$

As stated previously, aortic dp/dt can be determined, from radial artery dp/dt, using transfer functions based upon invasive radial arterial pressure measurements (Pauca et al. 2001) or from "radially-placed" tonometers (Chen et al. 1997). Thus, clinically useful values, for pulse wave velocity, could be determined with a radial arterial catheter, to assess dp/dt, and an EDM to obtain values for distal aortic blood flow acceleration. Blood density, ρ, can also be found from direct measurements of either hemoglobin (Hb) or hematocrit (Hct) (Hinghofer-Szalkay 1986). These can be readily obtained. In addition, evaluation at $t = 0$, at the start of systole, would reduce the effects of reflected waves (Latham et al. 1985).

The Bramwell-Hill equation also describes pulse wave velocity (Milnor 1989; Bramwell and Hill):

$$v_{\mathrm{pw}} = \sqrt{\frac{\mathrm{Vol}}{\rho \cdot \mathrm{C_{cv}}}}. \tag{41}$$

In this application, Vol is an approximate or "characteristic" volume. The derivation of the Bramwell–Hill equation, using the Moens–Korteweg equation, is shown in Appendix C.

Substituting (39) into (41) and rearranging yields:

$$\rho \left[\frac{\frac{\mathrm{d}p}{\mathrm{d}t}|_{t=0}}{a(0)}\right]^2 C_{cv} = \mathrm{Vol}. \tag{42}$$

An EDM can also be used to assess "net" cardiovascular compliance so that:

$$C_{cv} = \frac{\mathrm{SV}}{\mathrm{PP}}. \tag{43}$$

where SV is stroke volume and PP is pulse pressure. Note that PP would have to be "corrected" for pulse augmentation (Davies et al. 2003) when derived from either a radial artery catheter or a noninvasive blood pressure cuff.

Thus, simultaneous use, of both a radial arterial catheter and an EDM, could yield clinically suitable values for aortic pulse wave velocity and "characteristic" volume. Real-time evaluation of these parameters may be beneficial in patient management.

Specifically, aortic pulse wave velocity may be useful during clinical management of those patients with aortic dissections or aortic trauma. Whereas real-time estimates of characteristic volume could be applicable in clinical fluid management decision making.

Aortic characteristic impedance, dp/dQ, or the time rate of change of pressure, dp/dt, divided by the time rate change of flow, dQ/dt, can also be estimated (Mitchell et al. 2003):

$$\frac{\mathrm{d}p}{\mathrm{d}Q} = \frac{\frac{\mathrm{d}p}{\mathrm{d}t}}{\frac{\mathrm{d}Q}{\mathrm{d}t}} = \frac{\rho v_{pw} a(t)}{A a(t)}. \tag{44}$$

Thus,

$$\frac{\mathrm{d}p}{\mathrm{d}Q} = \frac{\rho v_{pw}}{A}. \tag{45}$$

Furthermore,

$$\frac{\mathrm{d}p}{\mathrm{d}Q}|_{t=0} = \frac{\frac{\mathrm{d}p}{\mathrm{d}t}|_{t=0}}{\frac{\mathrm{d}Q}{\mathrm{d}t}|_{t=0}} = \frac{\frac{\mathrm{d}p}{\mathrm{d}t}|_{t=0}}{A a(0)}. \tag{46}$$

Note that (44–46) do not apply when $a(t) = 0$.

Estimating Stroke Work and Stroke Power

Left ventricular stroke work (Milnor 1989), SW, can be estimated by simultaneously combining peripherally drived aortic pressure measurements, $p(t)$, with EDM-based flow information, $Q(t)$:

$$\mathrm{SW} = \int_0^{\mathrm{FT}} p(t)Q(t)\mathrm{d}t = 1.4 \cdot A \cdot \int_0^{\mathrm{FT}} p(t)v(t)\mathrm{d}t. \tag{47}$$

The above integral can be evaluated using numerical techniques (Kreyszig 1999). Note the dimensionless constant 1.4 "corrects" distal aortic blood flow (See Appendix A). Thus *total* left ventricular stroke work could be approximated.

Left ventricular stroke power, SP (Milnor 1989), may also be examined:

$$\mathrm{SP} = \frac{\mathrm{SW}}{\mathrm{FT}}. \tag{48}$$

Correlations, to other measurements of SW and SP, may then be made (Bove et al. 1978). It should be noted that both SW and SP are assessments of left ventricular contractility (Milnor 1989; Noordergraaf 1978). This model also assumes normal cardiac valvular function.

Assessing Mean Blood Pressure During Systole

The spring, mass, and dashpot impedance resemblance can be used, with the logistic-based systolic model, to assess mean blood pressure during systole, $\bar{p}_{sys}$. The relative contributions, to $\bar{p}_{sys}$, from inertia, resistance, and elastance can then be evaluated:

$$\bar{p}_L = \frac{A \cdot L}{\mathrm{FT}} \cdot \int_0^{\mathrm{FT}} a(t)\mathrm{d}t \tag{49}$$

$$\bar{p}_R = \frac{A \cdot R}{\mathrm{FT}} \cdot \int_0^{\mathrm{FT}} v(t)\mathrm{d}t \tag{50}$$

$$\bar{p}_{\frac{1}{C}} = \frac{A}{\mathrm{FT} \cdot C} \cdot \int_0^{\mathrm{FT}} sd(t)\mathrm{d}t. \tag{51}$$

Thus:

$$\bar{p}_{\mathrm{sys}} = \frac{1}{\mathrm{FT}} \cdot \int_0^{\mathrm{FT}} p(t)\mathrm{d}t = \bar{p}_L + \bar{p}_R + \bar{p}_{\frac{1}{C}}. \tag{52}$$

Regarding inertia, the effects of acceleration, from $0 \le t \le t_{pv}$, are essentially negated by the effects of deceleration, from $t_{pv} \le t \le \mathrm{FT}$. Therefore, the *net effect* of inertia, on mean blood pressure during systole, is negligible. Although $\bar{p}_L \approx 0$, it should be noted that the effect of inertia, on *instantaneous* blood pressure during systole, is significant. Furthermore, $\bar{p}_R \approx \bar{p}_{\frac{1}{C}}$ See "A Numerical Example" section.

Overall, mean arterial blood pressure (MAP) can then be defined using $\bar{p}_{sys}$ and mean pressure during diastole, $\bar{p}_{dia}$:

$$\mathrm{MAP} = \frac{\mathrm{FT}}{RR} \cdot \bar{p}_{\mathrm{sys}} + \frac{RR - \mathrm{FT}}{RR} \cdot \bar{p}_{\mathrm{dia}}. \tag{53}$$

where RR is R to R interval.

A Numerical Example

This example is based upon typical values obtained with an EDM. Numerical values for the model are shown in Table 3. Furthermore, the following formula is also useful in comparing aortic and non-aortic contributions to inertia (Milnor 1989):

$$\text{aortic inertia} = \frac{\rho \hat{h}}{\pi \hat{r}^2}. \tag{54}$$

where ρ is blood density, $\hat{h}$ is an estimate of aortic length, and $\hat{r}$ is an estimate of overall aortic radius.

"Net" cardiovascular elastance can be examined with the EDM:

$$\text{''Net'' cardiovascular elastance} = \frac{\text{pulsepressure}}{\text{stroke volume}} = \frac{\mathrm{PP}}{\mathrm{SV}} = \frac{1}{C_{\mathrm{cv}}}. \tag{55}$$

where stroke volume is the product of aortic cross-sectional area, average velocity, and flow time. A dimensionless factor of 1.4 corrects for *total* SV. (See Appendix A).

The following matrix can be defined from the values in Table 3:

$$\begin{bmatrix} a(0) & v(0) & sd(0) \\ a(t_{\mathrm{pv}}) & v(t_{pv}) & sd(t_{pv}) \\ a(\mathrm{FT}) & v(\mathrm{FT}) & sd(\mathrm{FT}) \end{bmatrix} = \begin{bmatrix} 21.75 & 0 & 0 \\ 0 & 0.849 & 0.06 \\ -2.373 & 0 & 0.175 \end{bmatrix}. \tag{56}$$

So that:

$$\begin{bmatrix} a(0) & v(0) & sd(0) \\ a(t_{pv}) & v(t_{pv}) & sd(t_{pv}) \\ a(\mathrm{FT}) & \mathrm{v}(\mathrm{FT}) & sd(\mathrm{FT}) \end{bmatrix}^{-1} = \begin{bmatrix} 21.75 & 0 & 0 \\ 0 & 0.849 & 0.06 \\ -2.373 & 0 & 0.175 \end{bmatrix}^{-1} = \begin{bmatrix} 0.046 & 0 & 0 \\ -0.044 & 1.178 & -0.405 \\ 0.623 & 0 & 5.712 \end{bmatrix}. \tag{57}$$

The pressure matrix can then be defined:

$$\begin{bmatrix} p(0) \\ p(t_{pv}) \\ p(\mathrm{FT}) \end{bmatrix} = \begin{bmatrix} 8.665 \cdot 10^3 \\ 1.603 \cdot 10^4 \\ 1.2 \cdot 10^4 \end{bmatrix}. \tag{58}$$

These values for pressure, which are expressed in NMS units, correspond to $p(0) = 65$ mmHg, $p(t_{pv}) = 120$ mmHg, and $p(\mathrm{FT}) = 90$ mmHg.

Substituting into (19):

$$\begin{bmatrix} L \\ R \\ \frac{1}{C} \end{bmatrix} = \frac{1}{3.8 \cdot 10^{-4}} \left\{ \begin{bmatrix} 21.75 & 0 & 0 \\ 0 & 0.849 & 0.06 \\ -2.373 & 0 & 0.175 \end{bmatrix}^{-1} \begin{bmatrix} 8.665 \cdot 10^3 \\ 1.603 \cdot 10^4 \\ 1.2 \cdot 10^4 \end{bmatrix} \right\} = \begin{bmatrix} 1.048 \cdot 10^6 \\ 3.589 \cdot 10^7 \\ 1.945 \cdot 10^8 \end{bmatrix}. \tag{59}$$

A plot of both $v(t)$ and $p(t)$ is shown in Fig. 6. Note that $p(t)$ is based upon Eq. (11) and the values for L, R, and $1/C$ from (59). It should be realized that L, R, and $1/C$ correspond to values for inertia, resistance and elastance which are based on a "net effect" of aortic and non-aortic contributions. This is illustrated in Fig. 5.

The values for the Laplace transform coefficients: Φ, Ψ, Ω, and K are shown in Table 4. Using these, values

Table 3 Numerical values associated with the logistic-based systolic model

Term	Notation	Numerical value	Units	Equation(s)	Comments
Acceleration	α	7.25	m s^{-2}	(1, 2)	Acceleration term. See Fig. 2
Gain	β	3	Dimensionless	(2)	Gain. See Fig. 2
Inverse time constant	γ	6.154	s^{-1}	(2, 5)	Constant in exponential. See Fig. 2.
Blood density	ρ	1.06×10^3	kg m^{-3}	(38, 54, C.12, C.13)	See Appendix C
Distal aortic radius	r	1.1×10^{-2}	m		Used to determine distal aortic cross sectional area
Peak velocity	v_{peak}	0.849	m s^{-1}	(10)	Age-dependent
Average velocity	$\bar{V}$	0.486	m s^{-1}	(A.2)	See Appendix A
Stroke volume in distal aorta	SV_{aorta}	66×10^{-6}	m^3	(55, A.4)	See Appendix A
Distal aortic cross-sectional area	A	3.8×10^{-4}	m^2	(11, 15, A.4)	Determined using $A = \pi r^2$ where r is distal aortic radius
Flow time	FT	0.36	s	(1, 2, 5)	Left ventricle ejection time or flow time
Aortic inertia		6.6×10^5	kg m^{-4}	(54)	Based upon = 1.6 cm and = 0.5 m
Cardiovascular elastance	$\frac{1}{C_{CV}}$	8.45×10^7	N m^{-5}	(55)	Based upon a pulse pressure = 59 mmHg and SV = 93 ml.
Aortic characteristic resistance	TSVR	1.1×10^8	N s m^{-5}	See "Introduction" section	Based upon a MAP = 92 mmHg and CO = 6.7 L/min
Inertia	L	1.05×10^6	kg m^{-4}	(11, 19)	Inertia in mass-dashpot-spring model
Resistance	R	3.59×10^7	N s m^{-5}	(11, 19)	Resistance in mass-dashpot-spring model
Elastance	$1/C$	1.95×10^8	N m^{-5}	(11, 19)	Elastance in mass-dashpot-spring model
Time to peak pressure	t_{sys_peak}	0.143	s	(30, 35)	Occurs when $dp/dt = 0$
Pulse wave velocity	v_{pw}	6.157	m s^{-1}	(38, 39, 41)	See Appendix C
Characteristic volume	Vol	476×10^{-6}	m^3	(41, 42)	See Appendix C
Aortic characteristic impedance	dp/dQ	1.72×10^7	N s m^{-5}	(44–46)	Note that this represents *change* in pressure divided by *change* in flow
Stroke work	SW	1.42	J (N m)	(47)	See Appendix A
Stroke power	SP	3.95	Watts (N m s^{-1})	(48)	See Appendix A

for $p(t)$, derived from the inverse Laplace transform, are numerically identical to those of (11). From (29) or (35) dp/dt can be calculated as well as the time to peak pressure, t_{sys_peak}.

Using numerical integration techniques, the contributions of inertia, resistance, and elastance, to average pressure during systole, can be determined. The contribution of inertia is:

Table 4 Numerical values, and their associated units, for the Laplace transform coefficients (See "A Numerical Example" section)

Laplace coefficients	Numerical value	Units
ϕ	4.54×10^3	N m^{-2}
Ψ	1.7×10^5	N m^{-2} s^{-1}
Ω	4.97×10^4	N m^{-2} s^{-2}
K	-4.13×10^3	N m^{-2}

$$\bar{p}_L = \frac{A \cdot L}{FT} \cdot \int_0^{FT} a(t)dt = \frac{A \cdot L}{FT} \left[\int_0^{t_{pv}} a(t)dt + \int_{t_{pv}}^{FT} a(t)dt \right] \tag{60}$$

$$\bar{p}_L \approx 7.046 - 7.046 \approx 0 \text{ mmHg}. \tag{61}$$

Whereas the contribution of resistance is:

$$\bar{p}_R = \frac{A \cdot R}{FT} \cdot \int_0^{FT} v(t)dt = 49.76 \text{ mmHg}. \tag{62}$$

And elastance:

$$\bar{p}_{\frac{1}{C}} = \frac{A}{FT \cdot C} \cdot \int_0^{FT} sd(t)dt = 58.938 \text{ mmHg}. \tag{63}$$

Furthermore, aortic pulse wave velocity can be determined with (39):

$$\frac{\frac{dp}{dt}|_{t=0}}{\rho \cdot a(0)} = 6.157 \text{ m} \cdot \text{s}^{-1}. \quad (64)$$

Using (42), "characteristic volume" can also be examined:

$$\text{Vol} = \rho \left[\frac{\frac{dp}{dt}|_{t=0}}{a(0)} \right]^2 C_{cv} = 476 \cdot 10^{-6} \text{m}^3. \quad (65)$$

where $C_{cv} = \text{SV/PP} = 1.18 \times 10^{-8}$ m^5 N^{-1}.

Additional numerical values, and their associated units, are shown in Table 3.

Results

The values reported in this section, which are from prior studies, have been converted into NMS units. In addition, references regarding elastance have been converted from compliance: elastance = 1/compliance

It is instructive to compare the values, obtained from this modeling scheme, to those obtained through other models and to direct in vivo measurements.

Using a 4-element lumped parameter model, Segers et al. determined the inertial component to have a range of 1.33×10^6 to 3.33×10^7 kg m^{-4} in humans (Segers et al. 2001). Based on a 4-element windkessel model, Stergiopulos et al. reported inertia of 9.6×10^5 kg m^{-4} for a model of human aortic pressure and flow and 6.8×10^5 kg m^{-4} based upon human aortic measurements (Stergiopulos et al. 1999).

Based upon the spring, mass, and dashpot resemblance, an estimate of "systemic" inertia of 1.05×10^6 kg m^{-4} was found. Whereas, using an assumed "net" radius of 1.6 cm and an overall length of 0.5 m, aortic inertia was found to be 6.6×10^5 kg m^{-4} (See Table 3).

Liu et al. determined mean in vivo human aortic elastance to be 9.07×10^7N m^{-5} (Liu et al. 1989). While Soma et al. reported a value of 9.3×10^7N m^{-5} for "net" cardiovascular elastance (Soma et al. 1999). Similarly, using stroke volume and pulse pressure, de Simone reported a mean value of 9.13×10^7 N m^{-5} (deSimone et al. 1999). Using typical EDM parameters, a value for "net" elastance was found to be 8.45×10^7 N m^{-5} (See Table 3).

Based on the 4-element lumped parameter model, Segers et al. estimated the elastance of the "proximal large arteries" with a range of 2.05×10^7 to 3.33×10^8 N m^{-5} (Segers et al. 2001). Using a 4-element windkessel, Stergiopulos et al. reported their elastance parameter, in humans, to have a range of 5.27×10^7 to 1.09×10^8 N m^{-5} (Stergiopulos et al. 1999). Similarly, the logistic-based model demonstrated a value of 1.95×10^8 N m^{-5} (See Table 3).

It should be noted that the resistance term in the spring, mass, and dashpot resemblance is significantly smaller than TSVR. This happens as a function of the "series nature" of the model. Nonetheless, TSVR is estimated within a normal range of approximately 7.7×10^7 to 1.5×10^8 N s m^{-5}.

Mitchell et al. reported a mean value for aortic characteristic impedance, or dp/dQ, as 1.85×10^7 N s m^{-5} (Mitchell et al. 2003). Mitchell et al. also reported a "time to peak pressure" as 0.188 ± 0.046 s for normotensive females and 0.194 ± 0.048 s for normotensive males (Mitchell et al. 2003). In addition, this group also reported a carotid-femoral pulse wave velocity, v_{pw}, as 8.2 ± 2.3 m s^{-1} for normotensive females and 9.4 ± 2.8 m s^{-1} for normotensive males. It should be noted that carotid-femoral pulse wave velocity is an approximation of aortic pulse wave velocity.

Using the logistic-based systolic model, a value of dp/dQ was found to be 1.72×10^7 N s m^{-5} whereas a "time to peak pressure" was 0.143 s. A pulse wave velocity of 6.157 m s^{-1} was also shown (See Table 3).

Using the Bramwell–Hill relationship (See Appendix C) a value of 476×10^{-6} m^3 was found for characteristic volume. Using a cylindrical approximation of the aorta, with a radius of 1.6 cm and a length of 0.5 m, the approximate aortic volume would be 402×10^{-6} m^3.

Values for left ventricular stroke work and stroke power have been reported as 1.33 ± 0.21 J and 3.7 ± 0.62 W (Bove et al. 1978). Using the logistic-based systolic model, values of 1.42 J and 3.95 W were found (See Table 3).

Discussion

There should be little, if any, morbidity or mortality associated with hemodynamic monitoring. The EDM represents a milestone in improving quality and safety relative to the pulmonary artery occlusion catheter. Furthermore, the EDM yields continuous measurements of cardiac output, preload, and contractility. However, to calculate afterload, mean arterial blood pressure must be manually entered into the device.

This is because current EDMs are designed as "stand-alone" devices. By integrating esophageal Dopplers, with existing OR and ICU monitors, which would include radial arterial catheters and noninvasive blood cuffs, additional information could be available to the clinician. Thus, afterload and other hemodynamic parameters could be determined on a near-continuous basis.

Furthermore, with simultaneous pressure information, the net effect of aortic and non-aortic contributions to inertia, resistance and elastance could also be estimated in real time. This would be facilitated by direct measurements

of velocity, acceleration, and stroke distance from the EDM.

By applying the Bramwell–Hill equation, characteristic volume could be examined. This may prove to be useful as a "figure of merit" in clinical fluid management issues. Aortic characteristic impedance and pulse wave velocity could also be evaluated. The contributions of inertia, resistance, and elastance, to mean blood pressure during systole, may be examined. Finally, left ventricular stroke work and power can be estimated.

Additional clinical research would determine the value, as well as the limitations, of these EDM-generated hemodynamic parameters.

A logistic-based systolic model has also been developed to illustrate these additional measurements. This model also demonstrates how corrected flow time functions as an indirect measure of preload. Furthermore, the mass-dashpot-spring model also represents a useful representation for the aortic pressure-velocity relationship. Using straightforward linear algebra, in the time domain, reasonable estimates of inertia, resistance, and elastance can be made.

Clearly, the time has come to "merge" the EDM with existing operative and critical care monitoring devices.

Conclusion

The logistic-based systolic model, and its applications, illustrates some of the potential additional properties of the EDM. Specifically, the EDM may also be used to estimate the net effect of aortic and non-aortic contributions to inertia, resistance, and elastance. Furthermore, aortic pulse wave velocity, characteristic volume, and characteristic impedance could also be assessed. Estimates of left ventricular stroke work and power could be obtained.

This paper also illustrates the potential role of a logistic-based model in hemodynamic calculations. Furthermore, the mass-dashpot-spring representation, of the velocity–pressure relationship, lends itself to time-based solutions using linear algebra techniques. In addition, the role of corrected flow time, as a measure of preload and its contribution to changes in cardiac output and contractility, has been modeled.

As this device will be contributing a greater role in patient care, additional research will emerge thus further enhancing its clinical utility. This can be achieved by integrating the EDM with existing, as well as future, monitoring equipment. Additional research will also determine the limitations of this device and its overall function in critical patient management.

Appendix A

Determining Cardiac Output Using EDM Parameters (Boulnois and Pechoux 2000)

Stroke distance, in the distal aorta, SD_{aorta}, is determined from the integral of distal aortic blood flow velocity over flow time:

$$SD_{aorta} = \int_0^{FT} v(t)dt. \quad (A.1)$$

Note that the average velocity, of distal aortic blood flow $\bar{V}$, is:

$$\bar{V} = \frac{1}{FT}\int_0^{FT} v(t)dt. \quad (A.2)$$

Therefore, SD_{aorta} is equivalent to the product of average velocity and flow time:

$$SD_{aorta} = (\bar{V})(FT). \quad (A.3)$$

Stroke volume in the distal aorta is:

$$SV_{aorta} = (SD_{aorta})(A). \quad (A.4)$$

where A is the distal aortic cross-sectional area. Thus:

$$SV_{aorta} = (\bar{V})(A)(FT). \quad (A.5)$$

That portion of cardiac output, which flows through the distal aorta, is then:

$$CO_{aorta} = (SV_{aorta})(HR) = (\bar{V})(A)(FT)(HR). \quad (A.6)$$

In this application, flow time, FT, has units of seconds/beat and heart rate, HR, has units of beats/second. Therefore the product: FT × HR is dimensionless.

Total cardiac output is then:

$$CO = (\bar{V})(A)(FT)(HR)(1.4). \quad (A.7)$$

where 1.4 is a dimensionless constant which is based upon a linear regression analysis from clinical data (Boulnois and Pechoux 2000).

If distal aortic cross-sectional area is unknown, minute distance within the aorta, MD_{aorta}, can be defined as:

$$MD_{aorta} = (\bar{V})(FT)(HR). \quad (A.8)$$

Therefore, $MD_{aorta} = SD_{aorta} \cdot HR$. Thus, MD_{aorta} correlates with total cardiac output.

Appendix B

Determining Stroke Distance, in the Distal Aorta, by Integrating Aortic Blood Flow Velocity Over Time

Using the logistic-based systolic model:

$$sd(t) = \int v(t)\mathrm{d}t = \int \alpha\beta \mathrm{e}^{-\gamma t}\left[\left(1 - \frac{t}{\mathrm{FT}}\right)t\right]\mathrm{d}t \tag{B.1}$$

Separating the above so that $sd(t) = I_1 - I_2$—*constant of integration*:

$$I_1 = \int \alpha\beta \mathrm{e}^{-\gamma t} t\,\mathrm{d}t = \frac{(\gamma t \mathrm{e}^{-\gamma t} - \mathrm{e}^{-\gamma t})}{\gamma^2}\alpha\beta \tag{B.2}$$

$$I_1 = \frac{-(\gamma t + 1)}{\gamma^2}\alpha\beta \mathrm{e}^{-\gamma t} \tag{B.3}$$

$$I_2 = \int \alpha\beta \mathrm{e}^{-\gamma t}\frac{t^2}{\mathrm{FT}}\,\mathrm{d}t \tag{B.4}$$

$$I_2 = \frac{-(\gamma^2 t^2 \mathrm{e}^{-\gamma t} + 2\gamma t \mathrm{e}^{-\gamma t} + 2\mathrm{e}^{-\gamma t})}{\gamma^3}\frac{\alpha\beta}{\mathrm{FT}} \tag{B.5}$$

$$I_2 = \frac{(-(\gamma t)^2 - 2\gamma t - 2)}{\gamma^3}\frac{\alpha\beta}{\mathrm{FT}}\mathrm{e}^{-\gamma t} \tag{B.6}$$

$$I_1 - I_2 = \left(\frac{-(\gamma t + 1)}{\gamma^2} - \frac{(-(\gamma t)^2 - 2\gamma t - 2)}{\gamma^3 \mathrm{FT}}\right)\alpha\beta \mathrm{e}^{-\gamma t} \tag{B.7}$$

$$I_1 - I_2 = \frac{(-\gamma^2 t \mathrm{FT} - \gamma \mathrm{FT} + (\gamma t)^2 + 2\gamma t + 2)}{\gamma^3 \mathrm{FT}}\alpha\beta \mathrm{e}^{-\gamma t} \tag{B.8}$$

$$I_1 - I_2 = \left(\frac{-t}{\gamma} - \frac{1}{\gamma^2} + \frac{t^2}{\gamma \mathrm{FT}} + \frac{2t}{\gamma^2 \mathrm{FT}} + \frac{2}{\gamma^3 \mathrm{FT}}\right)\alpha\beta \mathrm{e}^{-\gamma t} \tag{B.9}$$

$$I_1 - I_2 = \left(\frac{\left(-1 + \frac{1}{\mathrm{FT}}\right)t}{\gamma} + \frac{\left(-1 + \frac{2t}{\mathrm{FT}}\right)}{\gamma^2} + \frac{2}{\gamma^3 \mathrm{FT}}\right)\alpha\beta \mathrm{e}^{-\gamma t} \tag{B.10}$$

The constant of integration is then chosen so that $sd(0) = 0$:

$$sd(t) = \left(\frac{\left(-1 + \frac{1}{\mathrm{FT}}\right)t}{\gamma} + \frac{\left(-1 + \frac{2t}{\mathrm{FT}}\right)}{\gamma^2} + \frac{2}{\gamma^3 \mathrm{FT}}\right)\alpha\beta \mathrm{e}^{-\gamma t} - \left(-1 + \frac{2}{\gamma \mathrm{FT}}\right)\frac{\alpha\beta}{\gamma^2}. \tag{B.11}$$

Thus:

$$\int v(t)\mathrm{d}t = sd(t) = \left[\left[\left(\frac{t}{\mathrm{FT}} - 1\right)t + \left(2\frac{t}{\mathrm{FT}} - 1\right)\frac{1}{\gamma} + \frac{2}{\mathrm{FT}\gamma^2}\right]\frac{\alpha\beta}{\gamma}\mathrm{e}^{-\gamma t}\right] - \left(-1 + \frac{2}{\gamma \mathrm{FT}}\right)\frac{\alpha\beta}{\gamma^2}. \tag{B.12}$$

Figure A1 is plot of $sd(t)$ which reveals the familiar sigmoid curve that is characteristic of the logistic function.

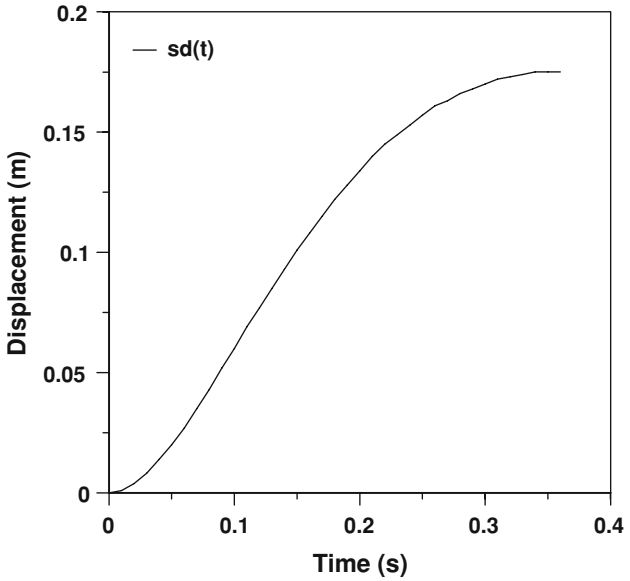

Fig. A1 A plot of stroke distance, sd(t), as a function of time. Note its sigmoid shape which is characteristic of the logistic function

Evaluating $sd(t)|_0^{\mathrm{FT}}$ yields $\mathrm{SD}_{\mathrm{aorta}} = sd(\mathrm{FT})$ since $\mathrm{sd}(0) = 0$:

$$\mathrm{SD}_{\mathrm{aorta}} = sd(\mathrm{FT}) - sd(0) = \left[\left(1 + \frac{2}{\mathrm{FT}\gamma}\right)\mathrm{e}^{-\gamma \mathrm{FT}} - \left(-1 + \frac{2}{\mathrm{FT}\gamma}\right)\right]\frac{\alpha\beta}{\gamma^2}. \tag{B.13}$$

Appendix C

Derivation of the Bramwell–Hill Equation (Bramwell and Hill 1922)

Tension, T, within the wall of a compliant cylinder can be described as:

$$T = \sigma h = r\Delta \mathrm{P}. \tag{C.1}$$

where σ is stress and h is wall thickness. It is assumed that h is small compared to radius, r. Furthermore, both internal and external radii are approximately equal and are represented as the constant r. ΔP represents the difference between external and internal wall pressures.

Therefore, wall stress is (Noordergraaf 1978):

$$\sigma = \frac{r\Delta P}{h}. \tag{C.2}$$

Strain, ε, is defined as:

$$\varepsilon = \frac{\Delta r}{r}. \tag{C.3}$$

Young's modulus, E, is:

$$E = \frac{\sigma}{\varepsilon} = \frac{\frac{r\Delta P}{h}}{\frac{\Delta r}{r}} = \frac{r^2 \Delta P}{h \Delta r}. \quad \text{(C.4)}$$

The change in radius, due to the change in pressure, can then be represented as:

$$\Delta r = \frac{r^2 \Delta P}{hE}. \quad \text{(C.5)}$$

Compliance is defined as the change in volume divided by the change in pressure:

$$C = \frac{\Delta \text{Vol}}{\Delta P} = \frac{\pi r_f^2 L_e - \pi r_i^2 L_e}{\Delta P} = \frac{\pi L_e (r_f^2 - r_i^2)}{\Delta P}. \quad \text{(C.6)}$$

where r_f is the final radius and r_i is the initial radius and L_e is the length of the compliant cylinder. Recognizing that $(r_f^2 - r_i^2)$ is the difference of two squares, (C.6) can then be expressed as:

$$C = \frac{\pi L_e (r_f + r_i)(r_f - r_i)}{\Delta P}. \quad \text{(C.7)}$$

Noting that $r_f + r_i \approx 2r$ and $r_f - r_i = \Delta r$, then (C.7) can be expressed as:

$$C = \frac{\pi L_e (2r)(\Delta r)}{\Delta P}. \quad \text{(C.8)}$$

Substituting (C.5) into (C.8) yields:

$$C = \frac{\pi L_e (2r)(r^2 \Delta P)}{hE \Delta P}. \quad \text{(C.9)}$$

Compliance can then be expressed as:

$$C = \frac{2 \cdot \text{Vol} \cdot r}{hE}. \quad \text{(C.10)}$$

Young's modulus can then be represented as:

$$E = \frac{2 \cdot \text{Vol} \cdot r}{hC}. \quad \text{(C.11)}$$

The Moens–Korteweg equation (Milnor 1989) relates pulse wave velocity, in a compliant cylinder, to its geometric and physical properties:

$$v_{pw} = \sqrt{\frac{Eh}{2\rho r}}. \quad \text{(C.12)}$$

Substituting (C.11) into (C.12) and simplifying yields the Bramwell–Hill equation ([Milnor 1989; Liu et al. 1989):

$$v_{pw} = \sqrt{\frac{\frac{2 \cdot \text{Vol} \cdot r}{hC} h}{2\rho r}} = \sqrt{\frac{\text{Vol}}{\rho C}}. \quad \text{(C.13)}$$

References

American Society of Anesthesiologists Task Force on Guidelines for Pulmonary Artery Catheterization. Practice Guidelines for Pulmonary Artery Catheterization. Anesthesiology. 2003;99(4):988–1014.

Atlas G. Can the esophageal Doppler monitor be used to clinically evaluate peak left ventricular dp/dt? Cardiovasc Eng Intl J. 2002;2(1):1–6

Atlas G, Mort T. Placement of the esophageal Doppler ultrasound monitor probe in awake patients. Chest. 2001;119:319.

Beltrami E. Mathematics for dynamic modeling. San Diego, CA: Academic Press; 1987.

Blacher J, Guerin AP, Pannier B, Marchais SJ, Safar ME, London GM. Impact of aortic stiffness on survival in end-stage renal disease. Circulation. 1999;99:2434–39.

Boulnois JLG, Pechoux T. Non-invasive cardiac output monitoring by aortic blood flow measurement with the Dynemo 3000. J Clin Monit Comput. 2000; 16:127–40.

Bove AA, Kreulen TH, Spann JF. Computer analysis of left ventricular dynamic geometry in man. Am J Cardiol. 1978;41(7): 1239–48

Bramwell JC, Hill AV. The velocity of the pulse wave in man. Proc R Soc Lond B Contain Paper Biol Charact. 1922;93(652):298–306.

Bulpitt CJ, Rajkumar C, Cameron JD. Vascular compliance as a measure of biological age. J Am Geriatr Soc. 1999;47(6):657–63.

Carney WI, Rheinlander HF, Cleveland RJ. Control of acute aortic dissection. Surgery. 1975;78:114–20.

Chen CH, Nevo E, Fetics B, Pak PH, Yin FCP, Maughan WL, Kass DA. Estimation of central aortic pressure waveform by mathematical transformation of radial tonometry pressure. Circulation. 1997;95:1827–36.

Dark PM, Singer M. The validity of trans-esophageal Doppler ultrasonography as a measure of cardiac output in critically ill adults. Intensive Care Med 2004;30:2060–66.

Davies JI, Band MM, Pringel S, Ogston S, Struthers AD. Peripheral blood pressure measurement is as good as applantion tonometry at predicting ascending aortic blood pressure. J Hypertens. 2003; 21:571–6.

De Hert SG, Robert D, Cromheecke S, et al. Evaluation of left ventricular function in anesthesized patients using femoral artery dP/dt(max). J Cardiothoracic Vasc Anesth. 2006;20(3):325–30.

deSimone G, Roman MJ, Koren MJ, Mensah GA, Ganau A, Devereux RB. Stroke volume/pulse pressure ratio and cardiovascular risk in arterial hypertension. Hypertension. 1999;33(3):800–5.

DiCorte CJ, Latham P, Greilich PE, Cooley MV, Grayburn PA, Jessen ME. Esophageal Doppler monitor determinations of cardiac output and preload during cardiac operations. Annl Thorac Surg. 2000;69(6):1782–6.

Dodd TEL. Nasal insertion of the oesophageal Doppler probe. Anaesthesia. 2002;57(4):412.

Domino KB, Bowdle TA, Posner KL, Spitellie PH, Lee LA, Cheney FW. Injuries and liability related to central vascular catheters: a closed claims analysis. Anesthesiology. 2004;100(6):1411–8.

DuBourg O, Jondeau G, Beauchet A, Hardy A, Bourdarias JP. Doppler-derived aortic maximal acceleration: a reliable index of left ventricular systolic function. Chest. 1993;103(4):1064–7.

English JD, Moppett IK. Evaluation of trans-oesophageal Doppler probe in awake patients. Anaesthesia. 2005;60:712–26.

Feldman LS, Anidjar M, Metrakos P, Stanbridge D, Fried GM, Carli F. Optimization of cardiac preload during laparoscopic donor nephrectomy: a preliminary study of central venous pressure versus esophageal Doppler monitoring. Surg Endosc. 2004; 18(3):412–6.

Gan TJ, Soppitt A, Maroof M et al. Goal-directed intraoperative fluid administration reduces length of hospital stay after major surgery. Anesthesiology. 2002;97(4):820–26.

Gardin JM, Davidson DM, Rohan MK, Butman S, Knoll M, Garcia R, Dubria S, Gardin SK, Henry WL. Relationship between age, body size, gender, and blood pressure and Doppler flow

measurements in the aorta and pulmonary artery. Am Heart J. 1987;113:101–9.
Groenink M, de Roos A, Mulder BJM, Spaan JAE, van der Wall EE. Changes in aortic distensibility and pulse wave velocity assessed with magnetic resonance imaging following beta-blocker therapy in the Marfan syndrome. Am J Cardiol. 1998;82(2):203–8.
Hinghofer-Szalkay H. Method of high-precision microsample blood and plasma densitometry. J Appl Physiol. 1986;60(3):1082–8.
Hopkins KD, Lehmann ED, Gosling RG (1994) Aortic compliance measurements: a non-invasive indicator of atherosclerosis? Lancet. 1994;343(8911):1447.
Hsieh KS, Chang CK, Chang KC, Chen HI. Effect of loading conditions on peak aortic flow velocity and its maximal acceleration. Proc Natl Sci Council Repub China B Life Sci. 1991; 15(3):165–70.
Kreyszig E. Advanced engineering mathematics. 8th ed. New York, NY: John Wiley & Sons; 1999.
Kumar A, Anel R, Bunnell E, et al. Preload-independent mechanisms contribute to increased stroke volume following large volume saline infusion in normal volunteers: a prospective interventional study. Critic Care. 2004; 8(3):R128–36.
Lafanechere A, Albaladejo P, Raux M, et al. Cardiac output measurements during infrarenal aortic surgery: echo-esophageal Doppler versus thermodilution catheter. J Cardiothor Vasc Anesth. 2006;20(1):26–30.
Latham RD, Westerhof N, Sipkema P, et al. Regional wave travel and reflections along the human aorta: a study with six simultaneous micromanometric pressures. Circulation. 1985;72:1257–69.
Lehmann ED. Clinical value of aortic pulse-wave velocity measurement. Lancet. 1999;354(9178):528–9.
Levy N. Extending the oesophageal Doppler into the perioperative period. Anaesthesia 2001;56(11):1123–24.
Liu Z, Ting CT, Zhu S, Yin FCP. Aortic compliance in human hypertension. Hypertension. 1989;14:129–36.
Madan AK, UyBarreta VV, Aliabadi-Wahle S, Jesperson R, Hartz RS, Flint LM, Steinberg SM. Esophageal Doppler ultrasound monitor versus pulmonary artery catheter in the hemodynamic management of critically ill surgical patients. J Trauma Injury Infect Critic Care. 1999;46(4):607–11.
Matsubara H, Araki J, Takaki M, Nakagawa ST, Suga H. Logistic characterization of left ventricular isovolumic pressure-time curve. Jpn J Physiol. 1995;45:535–52.
McEniery CM, Wallace YS, Maki-Petaja K, et al. Increased stroke volume and aortic stiffness contribute to isolated systolic hypertension in young adults. Hypertension 2005;46(1):221–6.
Milnor WR. Hemodynamics. 2nd ed. Baltimore, MD: Williams & Wilkens; 1989.
Mitchell GF, Lacourciere Y, Ouellet JP, et al. Determinants of elevated pulse pressure in middle-aged and older subjects with uncomplicated systolic hypertension. The role of proximal aortic diameter and the aortic pressure-flow relationship. Circulation 2003;108:1592–8.
Mowat DH, Haites NE, Rawles JM. Aortic blood velocity measurement in healthy adults using a simple ultrasound technique. Cardiovasc Res. 1983;17(2):75–80.
Nichols W, O'Rourke MF. McDonald's blood flow in arteries. 5th ed. London, UK: Hodder Arnold; 2005.
Noordergraaf A. Circulatory system dynamics. New York, NY: Academic Press; 1978.
Pauca AL, O'Rourke MF, Kon ND. Prospective evaluation of a method for estimating ascending aortic pressure from the radial artery pressure waveform. Hypertension. 2001;38:932–7.
Poeze M, Ramsay G, Greve JW, Singer M. Prediction of postoperative cardiac surgical morbidity and organ failure within 4 hours of intensive care unit admission using esophageal Doppler ultrasonography. Critic Care Med. 1999;27(7):1288–94.
Polanczyk CA, Rohde LE, Goldman L, Cook EF, Thomas EJ, Marcantonio ER, Mangione CM, Lee TH. Right heart catheterization and cardiac complications in patients undergoing noncardiac surgery. JAMA. 2001;286(3):309–14.
Prokop EK, Palmer RF, Wheat MW. Hydrodynamic forces in dissecting aneurysms. Circ Res. 1970;27:121–7.
Roeck M, Jakob SM, Boehlen T, et al. Change in stroke volume in response to fluid challenge: assessment using esophageal Doppler. Intensive Care Med. 2003;29:1729–35.
Rogers WJ, Hu YL, Coast D, Vido DA, Kramer CM, Pyretiz RE, Reichek N. Age-associated changes in regional aortic pulse wave velocity. J Am Coll Cardiol. 2001;38:1123–9.
Rothenberg DM, Tuman KJ. Pulmonary artery catheter: what does the literature actually tell us? Intl Anesthesiol Clin. 2000;38(4): 171–87.
Sandham JD, Hull RD, et al. A randomized, controlled trial of the use of pulmonary-artery catheters in high-risk surgical patients. NEJM. 2003;348(1):5–14.
Schertel ER. Assessment of left-ventricular function. Thorac Cardiovasc Surg. 1998;46(Suppl 2):248–54.
Segers P, Qasem A, De Backer T, Carlier S, Verdonck P, Avolio A. Peripheral "Oscillatory" compliance is associated with aortic + augmentation index. Hypertension. 2001;37:1434–9.
Seoudi HM, Perkal MF, Hanrahan A, Angood PB. The esophageal Doppler monitor in mechanically ventilated surgical patients: does it work? J Trauma Injury Infect Critic Care. 2003;55(4):720–6.
Singer M, Bennett ED. Noninvasive optimization of left ventricular filling using esophageal Doppler. Critic Care Med. 1991;19(9): 1132–7.
Singer M, Allen MJ, Webb AR, Bennett ED. Effects of alteration in left ventricular filling, contractility, and systemic vascular resistance on the ascending aortic blood velocity waveform of normal subjects. Crit Care Med 1991;19:1138–45.
Soma J, Aakhus S, Dahl K, Widerøe TE, Skjærpe T. Total arterial compliance in ambulatory hypertension during selective β_1 adrenergic receptor blockade and angiotensin-converting enzyme inhibition. J Cardiovasc Pharmacol. 1999;33(2):273–9.
Stergiopulos N, Westerhof BE, Westerhof N. Total arterial inertance as the fourth element of the windkessel model. Am J Physiol. 1999;276(Heart Circ Physiol 45):H81–8.
Sugawara M, Senda S, Katayama H, Masugata H, Nishiya T, Matsuo H. Noninvasive estimation of left ventricular Max(dP/dt) from aortic flow acceleration and pulse wave velocity. Echocardiography. 1994;11:377–84.
The National Heart, Lung, and Blood Institute Acute Respiratory Distress Syndrome (ARDS) Clinical Trials Network. Pulmonary-artery versus central venous catheter to guide treatment of acute lung injury. NEJM. 2006;354(21):2213–23.
Valtier B, Cholley BP, Belot JP, et al. Noninvasive monitoring of cardiac output in critically ill patients using transesophageal Doppler. Am J Respir Crit Care Med. 1998;158:77–83.
Vignon P. Hemodynamic assessment of critically ill patients using echocardiography Doppler. Curr Opin Critic Care. 2005;11(3): 227–34.
Vincent JL, Dhainaut JF, Perret C, Suter P (1998) Is the pulmonary artery catheter misused? A European view. Critic Care Med. 1998;26(7):1283–7.
Wallmeyer K, Wann LS, Sagar KB, Kalbfleisch J, Klopfenstein HS. The influence of preload and heart rate on Doppler echocardiographic indexes of left ventricular performance: comparison with invasive indexes in an experimental preparation. Circulation. 1986;74:181–6.
Warzawski RC, Deye AN, et al. Early use of the pulmonary artery catheter and outcomes in patients with shock and acute respiratory distress syndrome: a randomized controlled trail. JAMA. 2003;290(20):2713–20.